How motion trajectory affects energy extraction performance of a biomimic energy generator with an oscillating foil?

Qing Xiao [a], Wei Liao [b,d,*], Shuchi Yang [c], Yan Peng [d]

[a] Department of Naval Architecture and Marine Engineering, University of Strathclyde, Glasgow G4 0LZ, UK
[b] National Institute of Aerospace, Hampton, VA 23666, USA
[c] ZONA Technology, Inc., Scottsdale, AZ 85258, USA
[d] Department of Mathematics and Statistics, Old Dominion University, Norfolk, VA 23529, USA

ABSTRACT

A non-sinusoidal trajectory profile is proposed for the oscillating hydrofoil in the energy generators instead of conventional sinusoidal plunging/pitching motions to seek better energy extraction performance. The novel profile is achieved by combining a specially designed trapezoidal-like pitching motion with a sinusoidal plunging motion and investigated numerically on its output energy coefficient and total output efficiency. Through an adjustable parameter β, the pitching profile can be altered from a sinusoidal ($\beta = 1.0$) to a square wave ($\beta \to \infty$). In this work, a series of β ranging from 1.0 to 4.0 are investigated to examine the effect of combined motion trajectory on the energy extraction performance. The study encompasses the Strouhal numbers (St) from 0.05 to 0.5, nominal effective angle of attacks α_0 of 10° and 20° and plunging amplitude h_0/c of 0.5 and 1.0. Numerical results show that, for different β pitching motions, a larger α_0 always results in a higher extraction power C_{op} and total efficiency η_T. Compared with the sinusoidal motion ($\beta = 1$), significant increment of C_{op} and η_T can be observed for $\beta > 1$ over a certain range of St. The investigation also shows that there exists an optimal pitching profile which may increase the output power coefficient and total output efficiency as high as 63% and 50%, respectively, over a wide range of St. Detailed examination on the computed results reveal that, the energy extraction performance is determined by the relative ratio of the positive and negative contributions from the different combination of lift force, momentum and corresponding plunging velocity and pitching angular velocity, all of which are considerably affected by β.

© 2011 Elsevier Ltd. All rights reserved.

1. Introduction

The use of renewable energy, originated from natural resources such as wave, sunlight, tides and hydro, is being extensively explored. Among these renewable energies, marine current stream and tidal energy show a number of merits over others as it is predictable unlike wind energy being respondent to the random effects of weather system [1].

Tidal current energy is conventionally extracted through the deployment of turbine energy converters which are based on the rotational motion of blades [1,2]. In the past decade, marine current turbines have been growing up to a major industry, with a number of turbine farms having been constructed. The erection of these fixed marine turbine farms in ocean [2], however, has encountered some criticism for the supposed impact that they have on the environment, for example, they take up excessive amounts of space, become a danger to local wildlife, and require an average velocity of 5–7 knots to be financially viable, while the vast majority of currents flow at lower speeds [3].

In nature, many animals (aquatic animals, insects and birds) exploit energy directly from the fluid around them by controlling and maneuvering their bodies' locomotion via oscillation mechanism either actively and/or passively [4]. For example, tuna, dolphin and shark exhibit excellent hydrodynamic performance with high cruising speed, high efficiency and low noises by extracting water energy through their tail and/or fin's flapping motion. Recently, inspired by this biological ability, a new class of energy-harvesting prototype typified with unsteady, oscillation motions has been developed [2,3,5,6]. Notable examples are an oscillating marine current energy converter [3,5] and a flutter windmill [6] for wind

* Corresponding author. National Institute of Aerospace, Hampton, VA 23666, USA. Tel.: +1 757 8645042; fax: +1 757 3256979.
E-mail addresses: qing.xiao@strath.ac.uk (Q. Xiao), wliao@nianet.org (W. Liao), shuchi@zonatech.com (S. Yang), ypeng@odu.edu (Y. Peng).

energy harness. In principle, the water/wind kinetic energy is extracted to the mechanical energy and then transformed into electricity by the oscillation motion of device components, which imitates the propulsion and energy extraction mechanism adopted by the animals through the flapping motions of their tails, fins or wings. A schematic diagram for a typical energy extraction device based on a flapping wing is shown in Fig. 1. The rapid development of such devices has sparked the interest in understanding of their underlying fundamental aero/hydrodynamics.

The research on the hydro/aero behavior of oscillating based energy extraction phenomena is in its infancy although the concept can be dated back to 1981 [7]. Compared to its counterpart on oscillating propulsion [8–12], the study on flapping foils for energy extraction is very limited. Only in the past few years, the energy harness mechanism behind the oscillating foil has gradually attracted attention [13–20].

In the pioneer study by McKinney and DeLaurier [7], the ability of a harmonically oscillating wing, through combined pitching and plunging motions, to extract wind energy was investigated. It was shown that the output power was achievable and the efficiency was comparable to that of the rotational windmill. An earlier work was conducted by Davids [13] using experimental measurements and unsteady panel method. His numerical study on a NACA0012 foil showed that the total efficiency of energy extraction could be as high as 30% with optimized combination of plunging amplitude and frequency. Subsequently, Jones et al. [14,15] carried out a systematic numerical investigation by using an unsteady panel code coupled with a boundary layer algorithm. Their parametric studies covered a series of parameters ranging from thrust generation propulsion to power extraction. Given the fixed plunging amplitude and frequency, it was found that, if the pitching amplitude was increased to a sufficiently high value, the flow would change from energy consumption to power extraction. With various combinations of pitching and plunging, the condition for power extraction occurrence is that the pitching amplitude must exceed the plunging-induced angle of attack (AOA). A recent computational effort by Kinsey and Dumas [16] presented a mapping of power-extraction efficiency for an oscillating NACA0015 airfoil in the frequency and pitching amplitude domain. Through unsteady laminar-flow simulations using the commercial code FLUENT, they observed that, the maximum efficiency could go up to 34% with a foil plunging with one chord amplitude and pitching around one third of the chord within the domain of $0 < fc/U_\infty < 0.25$ and $0 < \theta_0 < 90°$. Here f is the oscillating frequency, c is the chord length, U_∞ is the far-stream velocity and θ_0 is the pitching amplitude.

An experimental investigation on a flapping foil was more recently conducted by Simpson et al. [17] By force/load measurement, they investigated the impact of Strouhal number ($St = fA/U_\infty$,
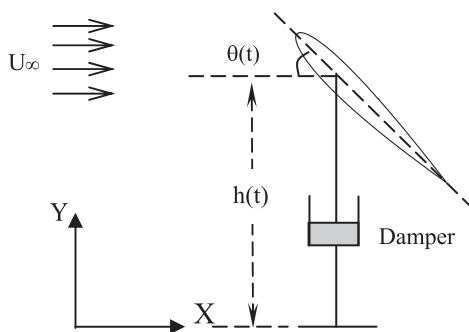
where A is the swept area of a flapping foil), maximum angle of attack, and aspect ratio on the power extraction efficiency of a NACA0012 foil. A maximum of hydrodynamic efficiency at 43% was found at the aspect ratio of 7.9, the Strouhal number of 0.4 and the maximum angle of attack of 34.37° with the phase angle difference of 90° between pitching and plunging.

Whilst some insights have been gained with these studies, by prescribing the pitching and plunging oscillation motions, the above numerical modeling decouples the interaction between oscillating device and its surrounding fluid. Therefore, they are concentrated on the hydrodynamic power only without taking into account the actuated power required for activating the device, which must be addressed by the coupled computation with fluid and dynamic response of device. Recently, some attempts have been made on this aspect [13–15]. Zhu and Peng [18,20] numerically studied, by using a Navier–Stokes solver, a novel approach to extract energy. In their approach, the pitching motion of the foil was prescribed, whilst the heaving motion, triggered by the unsteady time-dependent forces and moments induced by the oscillating pitching, was utilized for energy extraction. A positive net energy extraction was noted possibly only at low oscillating frequency. Similar approaches and results were obtained by Shimizu et al. [21] for the flapping wing study with its application in wind energy utilization.

Given the prescribed motion approach, it is worthy to note that, the foil in the above studies oscillates with no exception from sinusoidal plunging/pitching, as it is one of the simplest harmonic profiles. An interesting phenomena observed by previous research on propulsion foil [8–12] reveled that, under the condition of combined sinusoidal pitching/plunging, the climbing-up trend for thrust coefficient (C_t) and input power coefficient (C_{ip}) against St stops at a sufficiently high St and starts to diminish rapidly with further increasing St. This is strongly linked to the degradation of effective AOA (α_{eff}) from sinusoids at higher St. As we will show later, the similar behavior is observed on the output power coefficient (C_{op}) for the energy extraction case. As for the propulsion case, efforts were made initially by Hover et al. [10] through experiments, where α_{eff} was forced to be a cosine and then the plunging motion was derived. The propulsion performance was shown to be evidently improved at certain maximum effective angle of attack α_{max}. The derived plunging motion in such a case, however, becomes non-sinusoidal. A recent numerical attempt by Xiao and Liao [11] observed the similar tendency by modifying either pitching or plunging motion from a sinusoid. The computations also showed that the pitching modification yielded even better performance than that from the plunging adjustment. Such a phenomenon motivates us to investigate whether the power extraction performance of oscillating foil can be improved by replacing sinusoidal motions with non-sinusoidal oscillations.

In the present work, a non-sinusoidal trajectory is constructed by combining a specially proposed trapezoidal-like pitching motion with a sinusoidal plunging motion. By tuning an adjustable parameter β, one can gradually change the designed pitching profile from a sinusoid ($\beta = 1.0$) to a square wave ($\beta \to \infty$). This study is therefore concentrated on how motion trajectory affects power extraction performance. Computations will be conducted for a NACA0012 oscillating foil with a series of β values along with different oscillating frequency (f) and effective angles of attack α_{eff}.

2. Computational approach

2.1. Numerical method

In this study, time-dependent viscous flows around an oscillating NACA0012 foil for energy extraction purpose are simulated
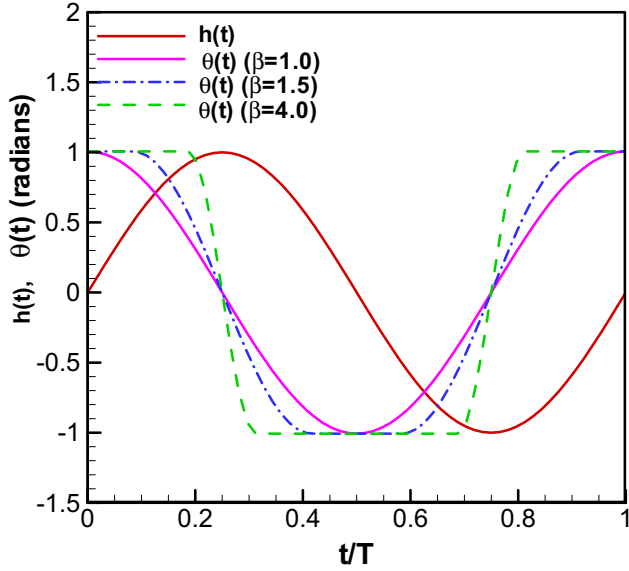

Fig. 1. A schematic diagram for a typical oscillating energy extraction device. (The damper represents the device of energy accumulation and storage, which is not considered yet in the present work.)

Fig. 2. Variation of instantaneous pitching $\theta(t)$ and plunging $h(t)$ profile in one period for different β. ($St = 0.35$, $h_0/c = 1.0$ and $\theta_0 = 58°$).
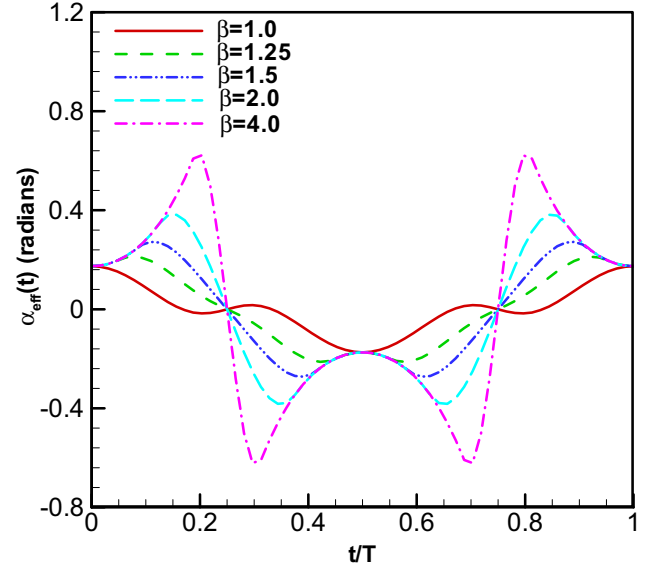

Fig. 3. Variation of instantaneous effective angle of attack profile in one period for different β. ($St = 0.35$, $h_0/c = 1.0$ and $\alpha_0 = 10°$).

by solving the unsteady compressible Navier–Stokes equations at a low Mach number. The details of the applied numerical methods were described in Xiao and Liao [11,12]. The code is based on a finite volume method with multi-block and multigrid features. A cell-centered finite volume method with a blend of second- and fourth-order artificial dissipations is used [22]. A dual time stepping method is selected to address unsteady problems.

The present computational code is solving the governing equations for unsteady compressible flows as follows:

$$\frac{\partial}{\partial t}\int_V W dV + \int_S (F_c - F_d)\cdot n\, dS = 0 \qquad (1)$$

The vector W contains the conservative variables.

$$W = \{\rho, \rho u, \rho v, \rho w, \rho E\}^T \qquad (2)$$

where ρ is the density, u, v, and w are the three Cartesian velocity components and E is the specific total energy of the flow, given by

$$E = \frac{p}{\rho(\gamma - 1)} + \frac{1}{2}\left(u^2 + v^2 + w^2\right) \qquad (3)$$

where γ is the gas specific hear ratio. The flux tensors F_c and F_d in Eq.(1) represent the inviscid convective fluxes and the diffusive fluxes, respectively.

The Reynolds number (Re) based on the far-stream velocity (U_∞) and chord length (c) is $Re = 10^4$ and laminar flows are assumed. It is well accepted that the flow can be treated as incompressible flow if the Mach number is less than 0.3 [23,24]. To avoid the effect of compressibility which might be caused by the compressible flow solver, all computations are conducted based on far-stream Mach number $Ma = 0.05$ and local Mach numbers in the flow field are kept being monitored during the computation to ensure that no Mach number is larger than 0.3.

2.2. Kinematic motion profile of foil

The foil oscillates with combined motions of plunging and pitching. A sinusoidal motion with amplitude of h_0 is imposed on the plunging as

$$h(t) = h_0 \sin(\omega t) \qquad (4)$$

while the foil pitches around one third of the chord from its leading edge with the following motion expression:

$$\theta = \begin{cases} \theta_0, & 0 < t \le \frac{\pi}{2\omega}\left(1 - \frac{1}{\beta}\right) \\[2mm] \theta_0 \sin\left(\beta\omega t + \pi\left(1 - \frac{\beta}{2}\right)\right), & \frac{\pi}{2\omega}\left(1 - \frac{1}{\beta}\right) < t \le \frac{\pi}{2\omega}\left(1 + \frac{1}{\beta}\right) \\[2mm] -\theta_0, & \frac{\pi}{2\omega}\left(1 + \frac{1}{\beta}\right) < t \le \frac{\pi}{2\omega}\left(3 - \frac{1}{\beta}\right) \\[2mm] \theta_0 \sin\left(\beta\omega t + \pi\left(2 - \frac{3\beta}{2}\right)\right), & \frac{\pi}{2\omega}\left(3 - \frac{1}{\beta}\right) < t \le \frac{\pi}{2\omega}\left(3 + \frac{1}{\beta}\right) \\[2mm] \theta_0, & \frac{\pi}{2\omega}\left(3 + \frac{1}{\beta}\right) < t \le \frac{2\pi}{\omega} \end{cases} \qquad (5)$$
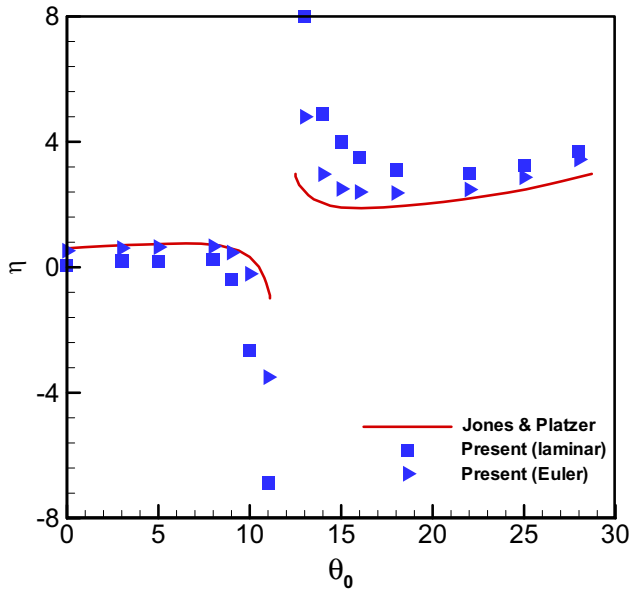
Fig. 4. Comparison of the computations on drag based efficiency for energy consumption/harnessing case (Jones and Platzer [14]) with $h_0/c = 0.2$, $\psi = 90°$ and $k = 1$.

The imposing of a non-sinusoidal profile on the pitching motion rather than the plunging is motivated by our earlier study on the oscillating foils for thrust generation [6], where we tested two cases with non-sinusoidal profiles imposed on either pitching or plunging while maintained another motion being sinusoid. Our results showed that a better improvement on thrust force and efficiency were achieved if such a change was applied on pitching.

The typical variation of instantaneous pitching amplitude $\theta(t)$ at different β over one oscillation period is shown in Fig. 2 with the conditions of $St = 0.35$, $h_0/c = 1.0$ and $\theta_0 = 58°$. As seen from Eq. (5) and Fig. 2, it is clear that $\beta = 1$ represents a sinusoidal pitching motion with 90° phase lag behind the plunging motion. At a fixed pitching amplitude θ_0, the profiles with β deviating from 1.0 display longer time interval during which $\theta(t) = \pm \theta_0$. This trend becomes more and more obvious with the increasing of β and gradually approaching a square wave.

2.3. Parameterization of energy extraction

For a foil oscillating problem, effective angle of attack $\alpha_{\text{eff}}(t)$ is a key parameter to quantify the combined effect of pitching and plunging. It is defined as:

$$\alpha_{\text{eff}}(t) = \alpha_h(t) + \theta(t) \tag{6}$$

where $\alpha_h(t)$ is the plunging induced angle of attack and equal to $(-\arctan(\dot{h}(t)/U_\infty))$

The effective AOA, which is time dependent, is therefore determined by

$$\alpha_{\text{eff}}(t) = -\arctan\left(\frac{\dot{h}(t)}{U_\infty}\right) + \theta(t) \tag{7}$$

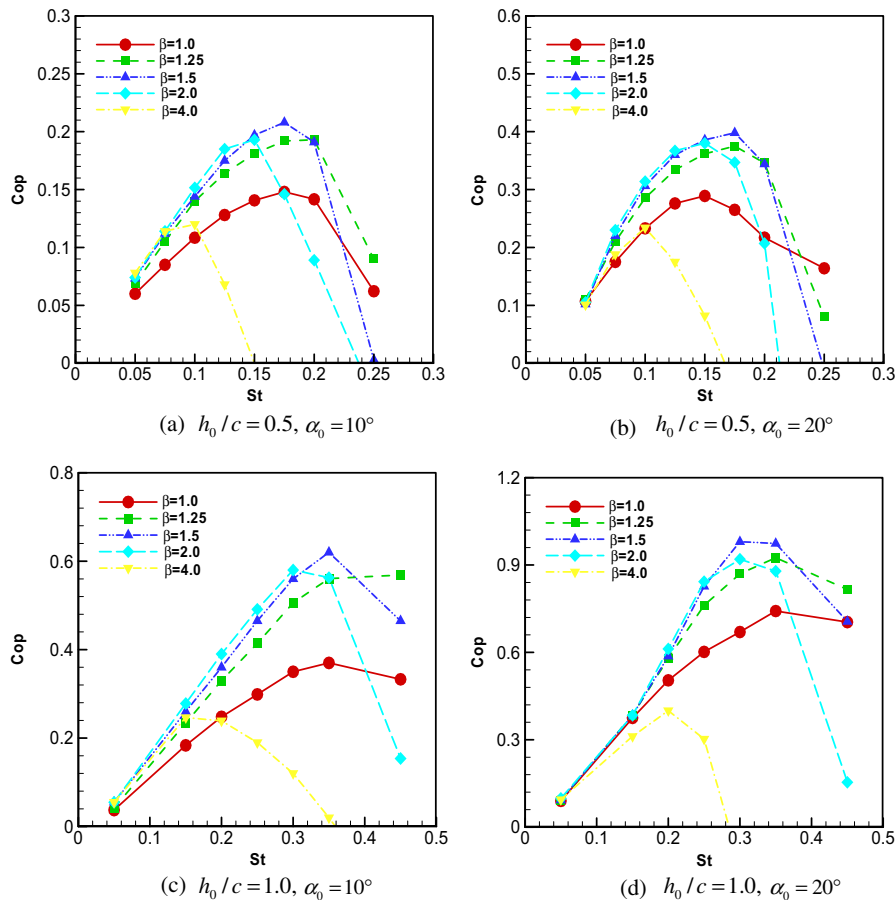

(a) $h_0/c = 0.5$, $\alpha_0 = 10°$

(b) $h_0/c = 0.5$, $\alpha_0 = 20°$

(c) $h_0/c = 1.0$, $\alpha_0 = 10°$

(d) $h_0/c = 1.0$, $\alpha_0 = 20°$

Fig. 5. Comparison of time-mean output power coefficient versus St for different β.

Table 1
Time-mean maximum output power coefficient C_{op} with $\beta = 1.0$.

	$h_0/c = 0.5$	$h_0/c = 1.0$
$\alpha_0 = 10°$	0.14	0.36
$\alpha_0 = 20°$	0.28	0.73

For simplicity, the nominal angle of attack (α_0), which is irrelevant of instantaneous time, is widely adopted in the flapping foil studies and defined as

$$\alpha_0 = -\arctan\left(\frac{\omega h_0}{U_\infty}\right) + \theta_0 \tag{8}$$

The instantaneous effective angles of attack $\alpha_{eff}(t)$ are illustrated in Fig. 3 for various β at a fixed nominal AOA $\alpha_0 = 10°$ with the plunging amplitude $h_0/c = 1.0$ and the oscillation frequency $St = 0.35$. As displayed, the peak effective AOA α_{max} grows up as β increases from 1.0 to 4.0 although the nominal AOA keeps a constant at $10°$.

To quantify the energy output, the time-mean power ($\overline{P}$) is calculated by integrating the instantaneous power (P) over one oscillation cycle as:

$$P = Y(t)\frac{dh(t)}{dt} + M(t)\frac{d\theta(t)}{dt} \tag{9a}$$

$$\overline{P} = \frac{1}{T}\int_0^T P\,dt \tag{9b}$$

where $Y(t)$ is the force component in y direction, $M(t)$ is the pitching moment and T is the oscillating period.

The non-dimensional instantaneous power coefficient C_{op} is defined as

$$C_{op} = P/\left(\frac{1}{2}\rho U_\infty^3 c\right) = \frac{2}{\rho U_\infty^3 c}\left[Y(t)\frac{dh(t)}{dt} + M(t)\frac{d\theta(t)}{dt}\right] \tag{10}$$

or

$$C_{op} = C_{p1} + C_{p2} = \frac{1}{U_\infty}\left[C_L(t)\frac{dh(t)}{dt} + C_M(t)\frac{d\theta(t)}{dt}\right] \tag{11}$$

where $C_L(t)$ is the instantaneous lift coefficient and $C_M(t)$ is the instantaneous momentum coefficient which are determined as follows:

$$C_L(t) = Y(t)/\frac{1}{2}\rho U_\infty^2 c \tag{12}$$

$$C_M(t) = M(t)/\frac{1}{2}\rho U_\infty^2 c \tag{13}$$

The time-mean power coefficient $\overline{C}_{op}$ over one cycle is calculated by the integration of instantaneous C_{op} over one cycle,

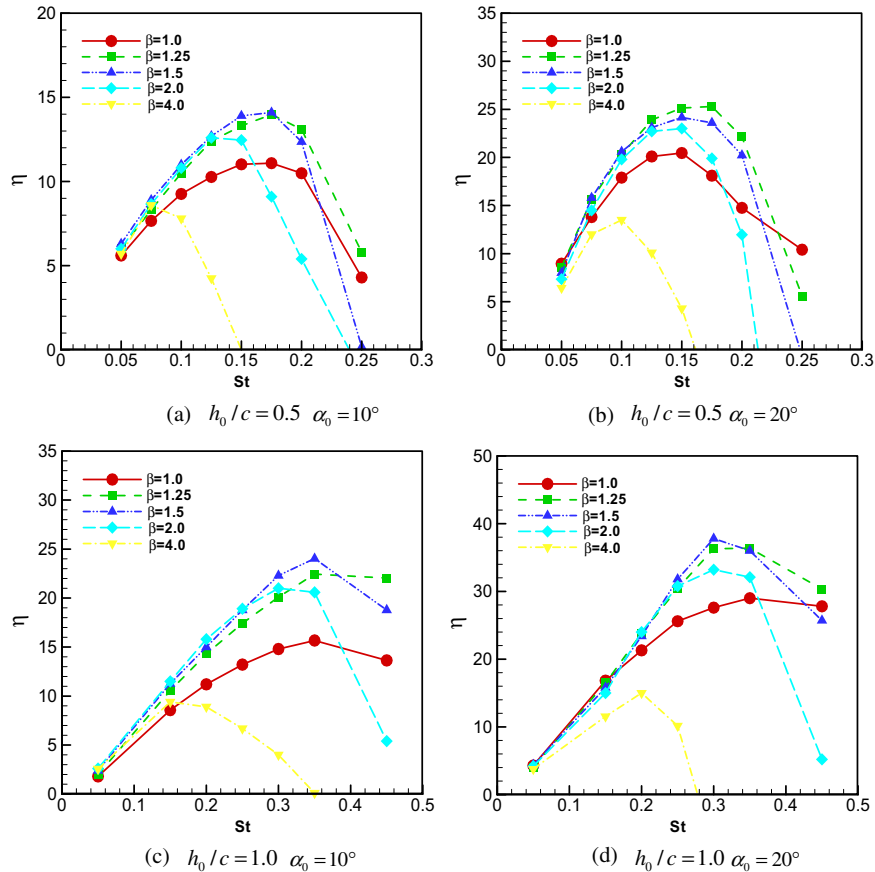$$\overline{C}_{op} = \frac{1}{T}\int_0^T C_{op}\,dt = \overline{P}/\left(\frac{1}{2}\rho U_\infty^3 c\right) \tag{14}$$

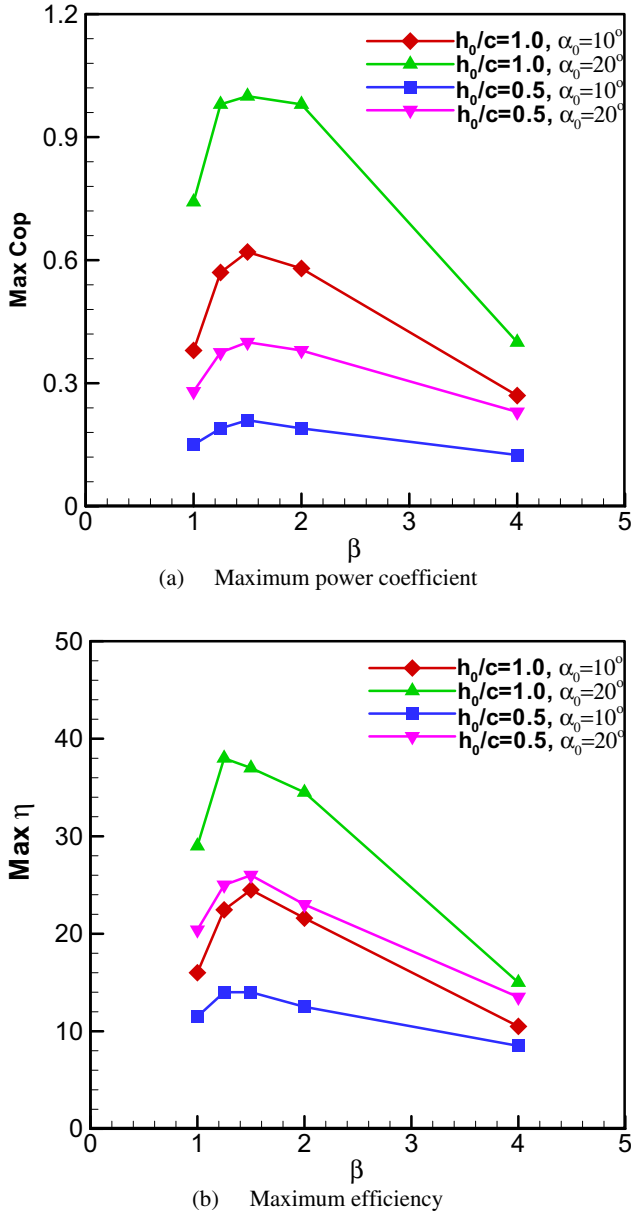Fig. 6. Comparison of time-mean efficiency versus St for different β.

(a)   Maximum power coefficient

(b)   Maximum efficiency

Fig. 7. Maximum time-mean output power coefficient and efficiency versus β.

or

$$\overline{C}_{op} = \overline{C}_{p1} + \overline{C}_{p2} = \frac{1}{U_\infty T} \left[\int_0^T C_L(t) \frac{dh(t)}{dt} dt + \int_0^T C_M(t) \frac{d\theta(t)}{dt} dt \right] \quad (15)$$

It can be clearly seen from Eqs. (11) and (15) that C_{p1} and $\overline{C}_{p1}$ represent the contribution to energy extraction from the lift while C_{p2} and $\overline{C}_{p2}$ denote that from the moment.

The total energy extraction efficiency η_T is defined as

$$\eta_T = \frac{\overline{P}}{\frac{1}{2}\rho U_\infty^3 A} = C_{op} \frac{c}{A} \quad (16)$$

where A is just the swept area of a flapping foil with $A = 2h_0$.

Table 2
Maximum difference of power coefficient, efficiency between $\beta = 1.0$ and $\beta > 1.0$.

C_{op} & η	$h/c = 0.5$	$h/c = 0.5$	$h_0/c = 1.0$	$h_0/c = 1.0$
	$\alpha_0 = 10°$	$\alpha_0 = 20°$	$\alpha_0 = 10°$	$\alpha_0 = 20°$
$C_{op}^{max}/C_{op}^{\beta=1}$ (at $\beta = 1.5$)	1.4	1.43	1.63	1.347
$C_{op}^{min}/C_{op}^{\beta=1}$ (at $\beta = 4.0$)	0.833	0.82	0.71	0.54
$\eta^{max}/\eta^{\beta=1}$	1.25 (at $\beta = 1.25$)	1.5 (at $\beta = 1.5$)	1.5 (at $\beta = 1.5$)	1.25 (at $\beta = 1.25$)
$\eta^{min}/\eta^{\beta=1}$ (at $\beta = 4.0$)	0.74	0.66	0.656	0.52

3. Results and discussions

3.1. Validation

The capability of the present code for simulating unsteady, viscous thrust-generated oscillating foil flows at low free-stream Mach numbers have been extensively validated and examined in Xiao and Liao [11,12]. The predicted instantaneous forces, time-average forces, thrust coefficients, efficiency and vortex structures agreed very well with other reported computational results and experimental data. To further validate the current code for oscillating foil energy extraction, numerical predictions are compared with simulation results from Jones and Platzer [14] for an oscillating NACA0012 foil.

To simulate the flow around an oscillating foil, a C-type mesh is used which extends 20 chords length in all directions. As shown in our previous work [11], the mesh dependence tests are also performed in this study (not present here for conciseness) with fine, medium and coarse grid number of 513 × 129, 385 × 65, and 193 × 33, respectively. Predicted flow field is well resolved with medium mesh, and thus most computations are conducted with the 385 × 65 mesh except for detailed vortices structure capturing cases, where the 513 × 129 mesh is used.

The efficiency based on the thrust coefficient ($\eta = C_p/C_t$) versus the pitching amplitude θ_0 at the given reduced frequency $k = 1$ and plunging amplitude $h_0/c = 0.2$ is shown in Fig. 4. Through the variation of θ_0, the oscillation foil ranges from energy consumption with $\eta < 1$ to energy extraction with $\eta > 1$. To compare the results by Jones and Platzer [14] with the panel method, our computations are conducted with both Euler solver and laminar solver. As indicated in Fig. 4, our Euler solutions are in good agreement with those from the panel method over the entire range from thrust generation (i.e., energy consumption) to energy extraction. The results by our laminar solver, however, are reasonably lower than those by the panel method due to the involvement of the viscous effect. The predicted discontinuity of η versus θ_0 curve is precisely agreeable with that of Jones and Platzer [14] at around $\theta_0 = 11.5°$ which indicates the oscillating foil changes from energy consumption to extraction at the given pitching amplitude.

Table 3
Maximum difference of St_c between $\beta = 1.0$ and $\beta > 1.0$.

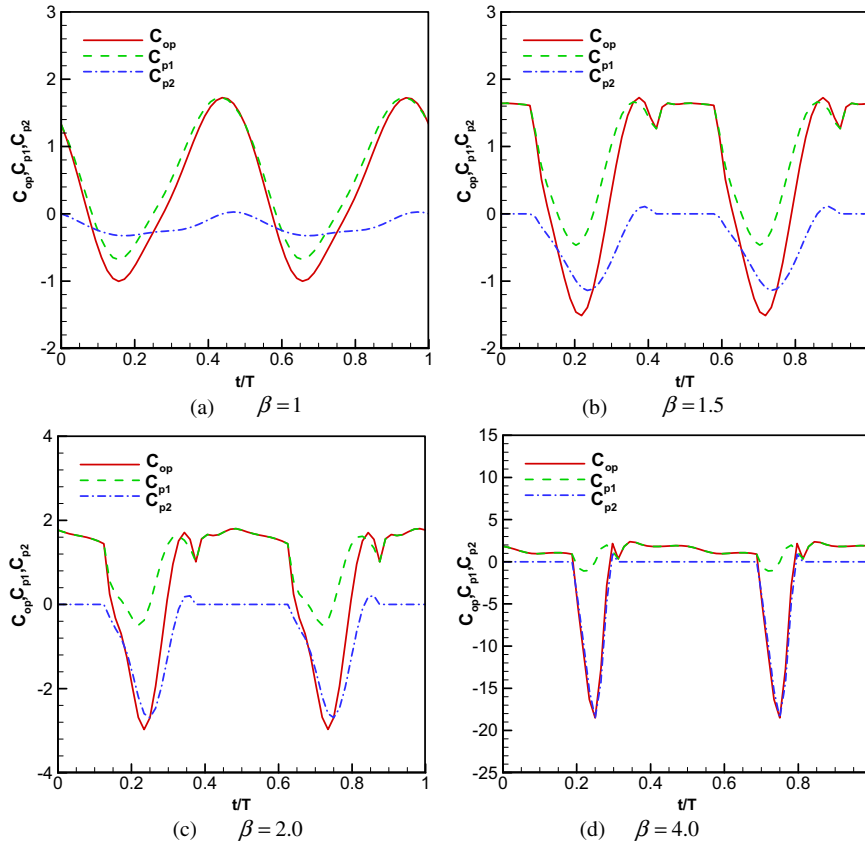| St	$h/c = 0.5$	$h/c = 0.5$	$h_0/c = 1.0$	$h_0/c = 1.0$
	$\alpha_0 = 10°$	$\alpha_0 = 20°$	$\alpha_0 = 10°$	$\alpha_0 = 20°$
$St_c^{max}/St_c^{\beta=1}$ (at $\beta = 1.25$)	1.17	1.17	1.28	1.347
$St_c^{min}/St_c^{\beta=1}$ (at $\beta = 4.0$)	0.57	0.66	0.43	0.57

Fig. 8. Instantaneous total output power coefficient (C_{op}), and two components Cp_1 and Cp_2 variation in one period with $St = 0.35$ and $\alpha_0 = 10°$.

3.2. Output power and efficiency

Two important parameters for the performance of energy extraction device are the power coefficient C_{op} and efficiency η_T defined in Eq. (15) and Eq. (16). We examine the effect of varying pitching motion profile, through the parameter β, on the energy extraction behavior. Five β of 1.0, 1.25, 1.5, 2.0 and 4.0 are studied with two plunging amplitude $h_0/c = 0.5$ and 1.0. To maintain two given nominal angle of attack $\alpha_0 = 10°$ and $\alpha_0 = 20°$, maximum pitching amplitude θ_0 is varied for various non-dimensional oscillation frequency St from 0.05 to 0.45.

The variation of time-mean output power coefficient C_{op} with St for different β varying from 1.0 to 4.0 is shown in Fig. 5(a) to (d) at $\alpha_0 = 10°$ and 20°, $h_0/c = 0.5$ and 1.0. In general, all curves for C_{op} versus St share some common features, e.g., the power coefficient initially increases with St until a critical point St_c, and afterward it decays with the further increasing St. This is true and irrelevant to the plunging amplitude h_0/c, nominal angle of attack α_0 and β. At a given St, the foil oscillating with larger h_0/c or α_0 generates much higher C_{op}. The peak C_{op} values for different h_0/c and α_0 with $\beta = 1.0$ (sinusoidal pitching) are summarized and listed in Table 1, which shows a monotonic growth of C_{op} with h_0/c and α_0. Similar observations are obtained for $\beta > 1.0$. From Eq. (8), it can be derived that both larger h_0/c at a given α_0 and larger α_0 at a given h_0/c are caused by higher θ_0. This means that more energy can be extracted with a higher pitching amplitude when the same oscillating frequency is applied to the foil. In terms of the critical St_c, at fixed β and α_0, the results with larger plunging amplitude present higher St_c, exhibiting that a wider range of high performance energy extraction is feasible for larger h_0/c.

Apart from above observations, some special features are revealed for different β. Clearly seen from Fig. 5(a) to (d), at a given St, compared to sinusoidal ($\beta = 1.0$) pitching, output powers significantly increase within a certain range of St by imposing the pitching profiles with $\beta > 1$. Among four cases tested here ($\beta = 1.25$, 1.5, 2.0 and 4.0), results obtained by $\beta = 1.25$ and 1.5 cover the widest St span with high power output. In fact, better performance is achieved at $\beta = 1.25$, 1.5, 2.0 than that at $\beta = 1.0$ from $St = 0.05$ to $St = 0.2$ for $h_0/c = 0.5$ and from St 0.05 to St 0.4 for $h_0/c = 1.0$, while the similar improvement only exists with $\beta = 4.0$ at very low St ($St = 0.1$). For $St > 0.1$ at $\beta = 4.0$, the output power is even less than that of the sinusoidal motion. Similar trends are observed in Fig. 6(a)–(d) on the energy output efficiency.

The effect of β on the peak C_{op} and η along each curve in Figs. 5 and 6 is recast into Fig. 7(a) and (b), respectively. Obviously, for fixed h_0/c and α_0, there exists an optimal β (i.e. $\beta = 1.25$ or $\beta = 1.5$) at which C_{op} and η reach their maxima. Too much increase of β causes dramatic degradation of the performance, like $\beta = 4.0$ case here. Refer to the instantaneous pitching profile plot in Fig. 2, this observation implies that increasing the time duration of $\theta(t) = \pm \theta_0$ (i.e. the profile becomes more flattened) can generally enhance the

Table 4
Time-mean C_{op}, C_{p1} and C_{p2} for different β at $St = 0.35$ and $\alpha_0 = 10°$.

β	C_{op}	C_{p1}	C_{p2}
1.0	0.36	0.55	−0.181
1.5	0.62	0.96	−0.34
2.0	0.563	1.13	−0.564
4.0	−0.842	1.23	−2.07

power output performance. However, there must be a limit for how much the flattened portion should be in one cycle. This is apparently relevant to St, nominal AOA and plunging amplitude h_0/c.

To quantitatively evaluate the effect of β on the energy extraction, we examine the critical Strouhal number St_c and the variation of the maxima of C_{op} and η over one cycle for $\beta = 1$ and $\beta > 1$ denoted by $C_{op}^{max}/C_{op}^{\beta=1}$, $C_{op}^{min}/C_{op}^{\beta=1}$, $\eta^{max}/\eta^{\beta=1}$ and $\eta^{min}/\eta^{\beta=1}$. Here, $C_{op}^{\beta=1}$ and $\eta^{\beta=1}$ represent the maxima of C_{op} and η, respectively, for

$\beta=1$ in one cycle; C_{op}^{max} and C_{op}^{min} are the largest and the smallest maxima of the C_{op} curves shown in Fig. 5 under different conditions, respectively; η_{op}^{max} and η_{op}^{min} are taken from the η curves in Fig. 6 in a similar way. The above ratios of the maxima for $\beta > 1$ and $\beta = 1$ are regarded as a key criteria here indicating whether the power output performance is improved and to what extend it does. Tables 2 and 3 summarize above quantities and associated β at which these values are reached. As seen from Table 2, the

(a) $\beta = 1.0$, C_L and dh/dt

(b) $\beta = 1.0$, C_M and $d\theta/dt$

(c) $\beta = 1.5$, C_L and dh/dt

(d) $\beta = 1.5$, C_M and $d\theta/dt$

(e) $\beta = 4$, C_L and dh/dt
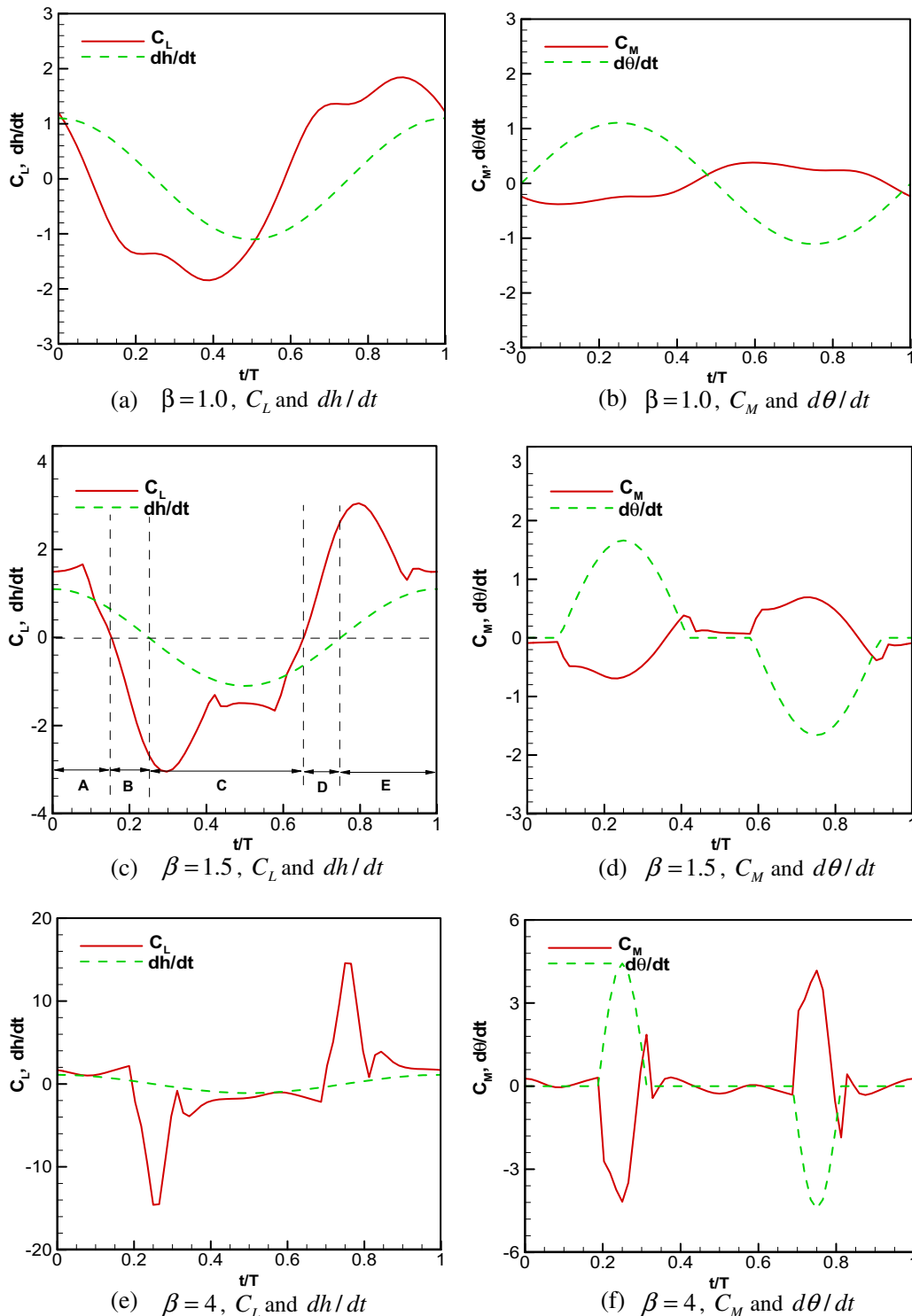
(f) $\beta = 4$, C_M and $d\theta/dt$

Fig. 9. Instantaneous lift coefficient (C_L), plunging velocity (dh/dt), momentum coefficient (C_M) and pitching velocity ($d\theta/dt$) variation in one period with $St = 0.35$ and $\alpha_0 = 10°$.

maximum output power occurs with $\beta = 1.5$ at $h_0/c = 1.0$ and $\alpha_0 = 10°$ with an increment of 63% over $\beta = 1.0$ case. However, the smallest power maximum is obtained with $\beta = 4.0$ at $h_0/c = 1.0$ and $\alpha_0 = 20°$ with a decay of 46% compared to $\beta = 1.0$. For $\beta = 1.5$, the maximal efficiency increases as high as 50% over $\beta = 1.0$ while 48% decreasing of efficiency is observed for $\beta = 4.0$ with $h/c = 1.0$ and $\alpha_0 = 20°$. The effect of β on St_c is presented in Table 3 where St_c^{max} are the maxima of the critical Strouhal numbers St_c for all parameters over one cycle and $St_c^{\beta=1}$ is the St_c for $\beta = 1$. The results show that the best improved performance in St_c are always achieved at $\beta = 1.25$ with the highest value of St_c extending to 1.347 times of that at $\beta = 1.0$ while the worst situation occurs at $\beta = 4.0$ again with St_c reducing to 43%~66% of that at $\beta = 1.0$. Clearly, the optimum pitching profile for the current tested case is $\beta = 1.5$ or $\beta = 1.25$ in terms of large power output as well as high efficiency.

3.3. Mechanism of energy output enhancement

To further analyze the mechanism of the effect of β on the power output, we examine the details of flow in terms of vorticity contours, foil surface pressure distribution and individual contributions from C_{p1} and C_{p2}, defined by Eq. (11), at $St = 0.35$ and $\alpha_0 = 10°$. Two β values with $\beta = 1.5$ and 4.0 are particularly selected because among all β, maximal positive increment for the peak C_{op} and η_t generally occurs with $\beta = 1.5$ while the worst situations in C_{op} and η_t are always observed with $\beta = 4.0$ as we discussed in previous sections.

3.3.1. Contributions from C_{p1} and C_{p2}

As shown in Eq. (11), the total output power is composed of C_{p1} and C_{p2}. By highlighting the contributions from above two parts, Fig. 8(a)–(d) plot the comparison of instantaneous C_{op}, C_{p1} and C_{p2}
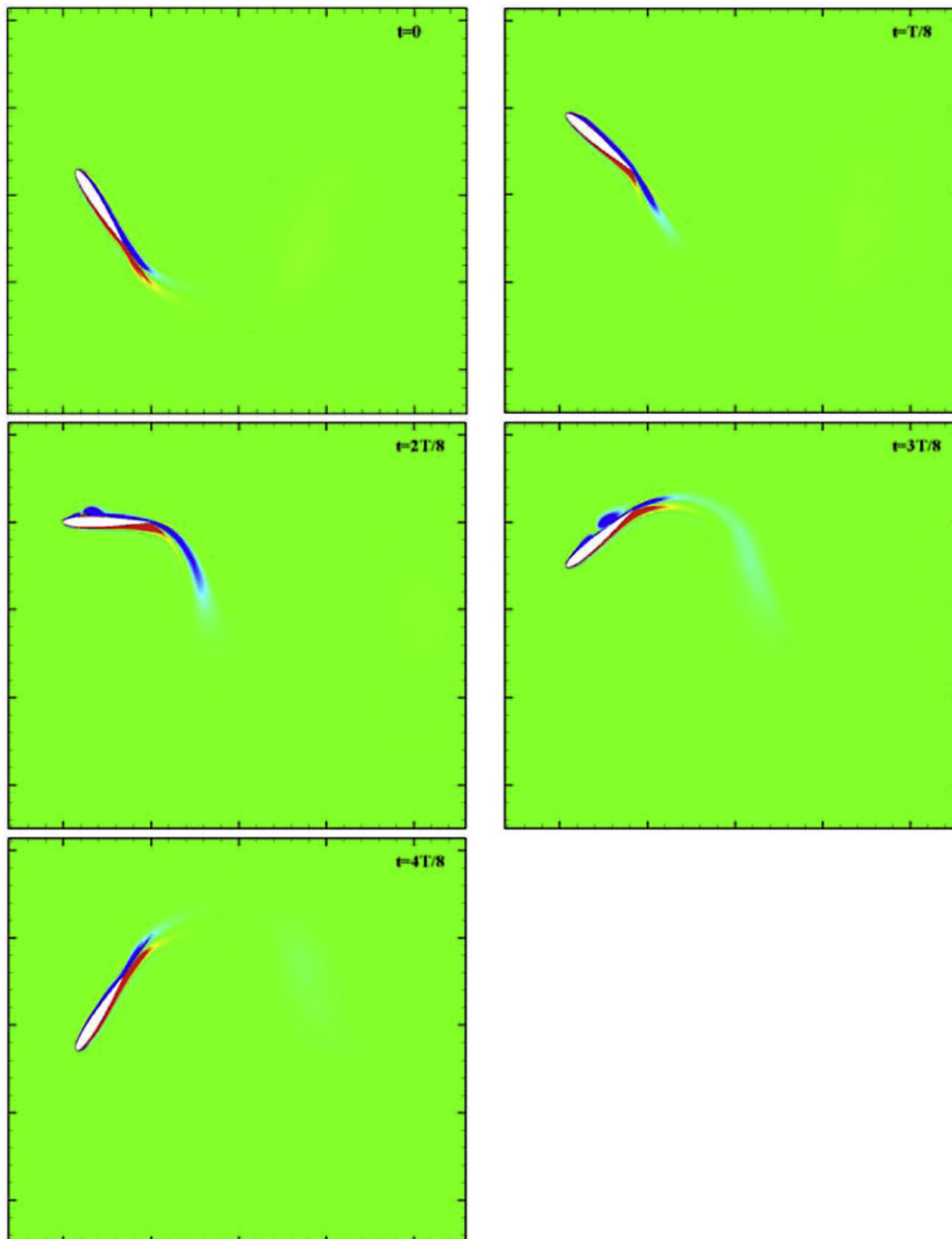

Fig. 10. Instantaneous vortex contour within one period at $\beta = 1.0$ with $St = 0.35$ and $\alpha_0 = 10°$.

variation over one period with $\beta = 1.0$ (*i.e.*, the sinusoid), $\beta = 1.5$, $\beta = 2.0$ and 4.0 at $St = 0.35$ and $\alpha_0 = 10°$. The time-averaged C_{op}, C_{p1} and C_{p2} over one cycle are summarized in Table 4 for quantitative comparison. Importantly to note that, generally C_{p2} contributes negative output power within most portion of the cycle whilst C_{p1} basically presents a positive output power over a cycle. The overall positive or negative output power C_p depends on whether C_{p1} or C_{p2} dominates the C_{op}

With the sinusoidal profile as shown in Fig. 8(a), contribution from C_{p2} is small compared to that from C_{p1} resulting in a positive output power C_{op}. In fact, $|C_{p2}|$ is one third of $|C_{p1}|$ for $\beta = 1.0$ as revealed in Table 4. The C_{op} versus t curve smoothly evolves along with the sinusoidal profile. However, the plots with $\beta = 1.5$, 2.0 and 4.0 display some new features. Comparing $\beta = 1.5$ in Fig. 8(b) to the sinusoid in Fig. 8(a), we can see that, the positive C_{p1} for $\beta = 1.5$ has higher peak values, and the portion of positive C_{p1} also extends

within the whole cycle, near its center part of the cycle ($0.35 < t/T < 0.55$) corresponding to the lengthened peak portion of the trapezoidal profile with $\theta(t) = \pm \theta_0$. Although the negative contribution of C_{p2} also increases at two time intervals around $t/T = 0.2$ and $t/T = 0.7$, due to the rapidly descending/ascending $d\theta/dt$ shown in Fig. 2, the contribution of C_{p1} to total C_p is still larger than that from C_{p2}, causing the overall time-mean C_p to increase. With the portion of $\theta(t) = \pm \theta_0$ further expanding at $\beta = 2.0$ and 4.0, C_{p2} becomes more and more dominant in the total C_{op} as shown in Fig. 8(c) and (d). Although the peak C_{p1} range is extended from $0.35 < t/T < 0.55$ with $\beta = 1.5$ to $0.25 < t/T < 0.7$ with $\beta = 4.0$, the positive contribution from C_{p1} to output power is lessened or canceled by the dramatically increased negative contribution from C_{p2}. As we can see from Fig. 8(d), with $\beta = 4.0$, the positive C_{p1} contribution is small compared to the negative C_{p2} contribution with $|C_{p1}| = 0.59|C_{p2}|$. The time-mean C_{op} in one cycle is therefore
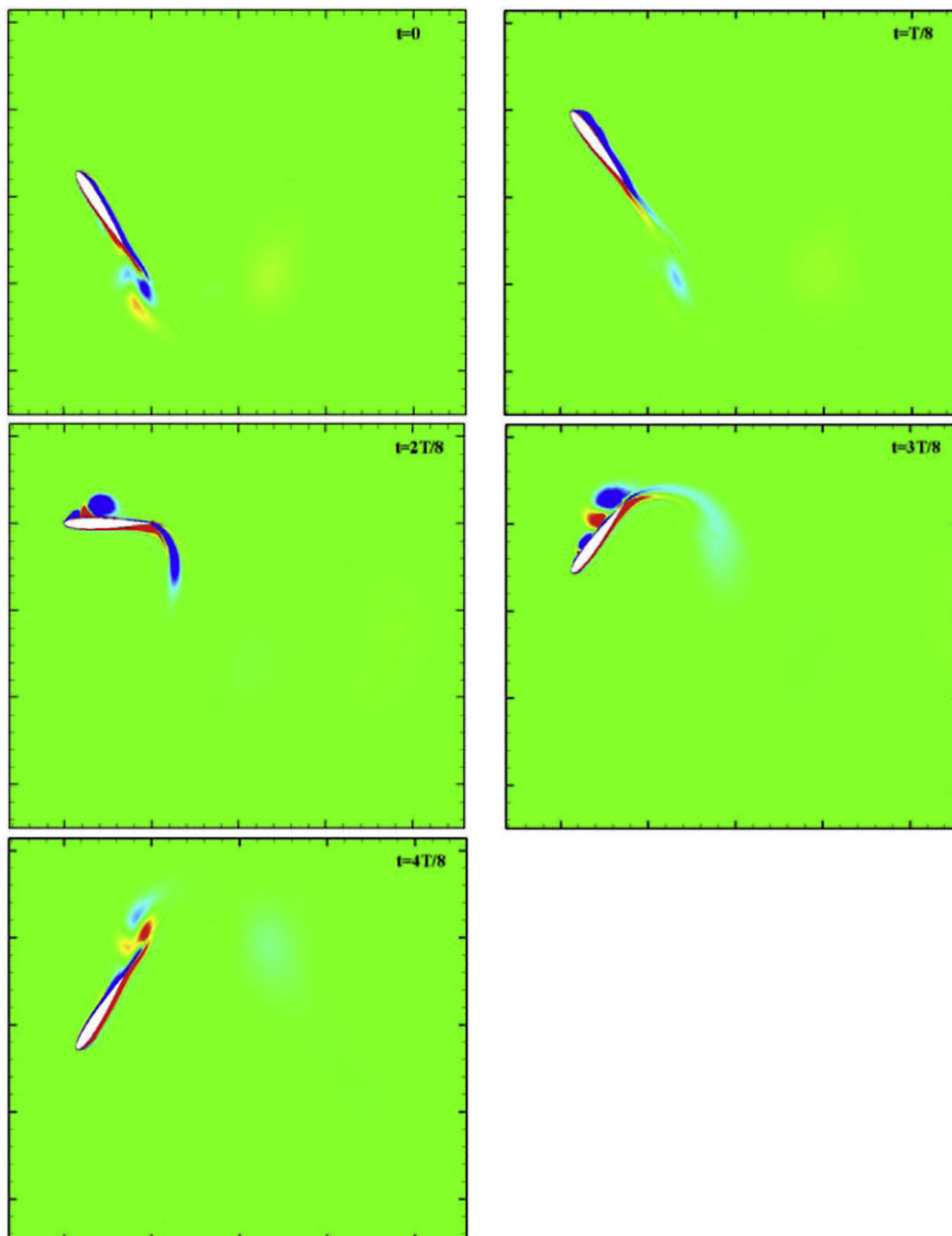

Fig. 11. Instantaneous vortex contour within one period at $\beta = 1.5$ with $St = 0.35$ and $\alpha_0 = 10°$.

dominated by the latter. Clearly, the conclusion from Fig. 8 is that, properly designed $\beta > 1.0$ pitching approach can be superior in that it increases the positive C_{p1} portion in one cycle, well controls the negative C_{p2} contribution to a low level, and therefore enhances the total output. From the definition of C_{p1} and C_{p2} as given by Eq. (16), we know that the former is fully determined by the lift coefficient C_L and plunging velocity dh/dt while the latter is computed by the product of the moment coefficient C_M and the pitching angular velocity $d\theta/dt$. The contribution of above four quantities to the overall C_{op} depends not only on their magnitudes but also their signs (determined by their directions) and even the portion of the time intervals in one cycle where the same or opposite sign appears. When C_L and dh/dt have the same sign as well as C_M and $d\theta/dt$, positive contribution is added to energy extraction, and otherwise, their effect on C_{op} will be negative. Such interesting behavior inspired us to further examine the variations of above four quantities over one cycle.

Fig. 9(a)–(f) display the evolution of C_L, dh/dt, C_M and $d\theta/dt$ in one cycle for $\beta = 1.0$, 1.5 and 4.0. We can examine the evolution of C_L and dh/dt by partitioning one cycle into five intervals A-E as depicted in the figure for $\beta = 1.5$. It is seen that C_L and dh/dt have the same sign at the intervals A, C and E and thus have positive contribution to C_{p1} while those at the intervals B and D have opposite sign, resulting in a negative contribution to C_{p1}. The time-mean $\overline{C}_{p1}$ over one cycle, therefore, considerably depends on the percentage of each interval in the one cycle. For $\beta = 1.5$, it is observed that the portion contributed by A, C and E is far beyond that of B and D, thus a positive $\overline{C}_{p1}$ is obtained and added in total $\overline{C}_{op}$. Similarly, the above analysis based on the five-interval partition in one cycle can also be applied to $\beta = 1.0$ and 4.0 (not displayed in the figures here). As seen, with the increase of β, intervals B and D become narrower and thus have less negative effect on $\overline{C}_{p1}$ and also $\overline{C}_{op}$. This can be proved by Fig. 8 in which one can easily find the corresponding parts of the intervals A to E on the C_{p1} plots.
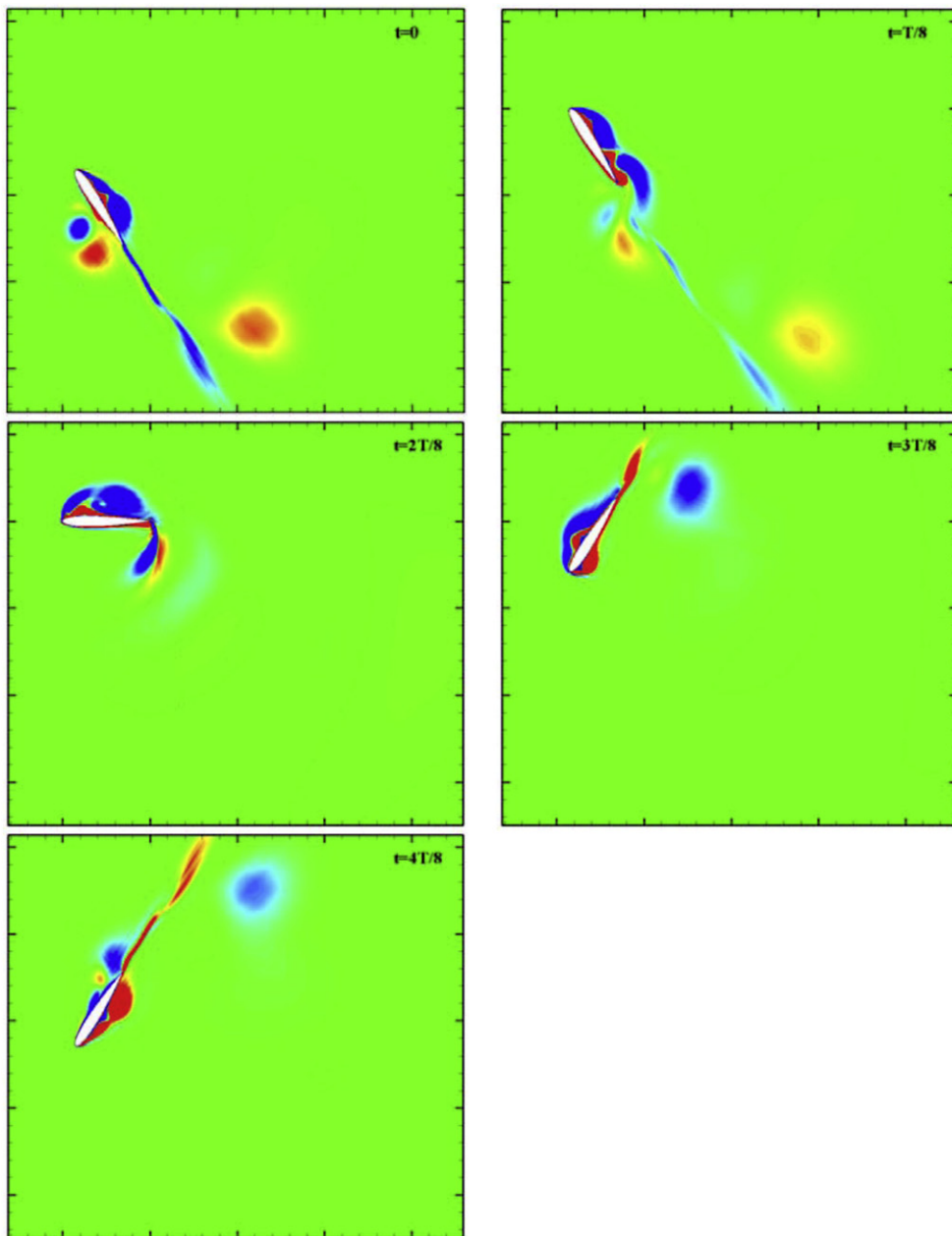

Fig. 12. Instantaneous vortex contour within one period at $\beta = 4.0$ with $St = 0.35$ and $\alpha_0 = 10°$.

Fig. 8 demonstrates that C_{p1} has large positive part and small negative one with β increasing.

The right three plots in Fig. 9 illustrate the profiles of C_M and $d\theta/dt$ in one cycle. It is clearly seen that the contribution of the moment coefficient is entirely different from that of lift coefficient. Instead of coexistence of partly same and partly opposite sign of C_L and dh/dt in one cycle, C_M and $d\theta/dt$ always have opposite sign provided that the pitching angular velocity ($d\theta/dt$) is not equal to zero. This indicates that the product of C_M and $d\theta/dt$ has significant negative contribution to total energy extraction (or $\overline{C}_{op}$) which can be clearly observed from the profile of C_{p2} shown in Fig. 8. It is noteworthy that, during the intervals of $\theta(t) = \pm \theta_0$ or $d\theta/dt = 0$, momentum coefficient C_M has also very small values. Obviously, their product has no contribution to energy output. At the same time, C_M have significant non-zero values during two intervals where the magnitudes of $d\theta/dt$ are not zero, especially with relatively large values. With β increasing, the portion of these two intervals shrinks as a result of enlarged time duration of $\theta(t) = \pm \theta_0$ as shown in Fig. 2. This is clearly reflected on the plot of two extreme cases with $\beta = 1$ and $\beta = 4$. In fact, for $\beta = 1$, the parts of $\theta(t) = \pm \theta_0$ where $d\theta/dt = 0$ shrink to two points on the $\theta(t)$ profile, and thus non-zero, opposite-sign C_M and $d\theta/dt$ occupy the entire cycle. However, these only occur during two narrow intervals from 0.2 T $< t <$ 0.35 T and 0.7 T $< t <$ 0.85 T for $\beta = 4$. Note that the magnitude of C_M increase dramatically with β in spite of the narrower intervals with $d\theta/dt \neq 0$ for large β,

Obviously, the results obtained above reinforce our earlier observation of C_L and C_M impact on C_{op}, i.e., generally C_L has positive effect on energy extraction while C_M makes negative contribution. These influences become much stronger with larger β, because C_L and C_M magnitudes increase apparently with β as well. However, the increase of β leads to the dramatic growth on the peak values of $d\theta/dt$ while never affects the values of dh/dt. Consequently, for a large enough β, the product of C_M and $d\theta/dt$ is far beyond that of C_L and dh/dt and thus, becomes dominant over the entire cycle for energy extraction process. This is why we observed in Fig. 8, the positive contribution to output power from C_{p1} is diminished or canceled by the rapidly increased negative contribution from C_{p2}.

3.3.2. Flow field and vortex structure

The variation of C_L and C_M during a cycle has significant influence on the output power as discussed above. The values of C_L and C_M are obviously subjected to the changes of surface forces which are in turn affected by the flow fields over the airfoil. Taking a close-up examination of near-body flow fields definitely helps our understanding on the mechanism of energy extraction.
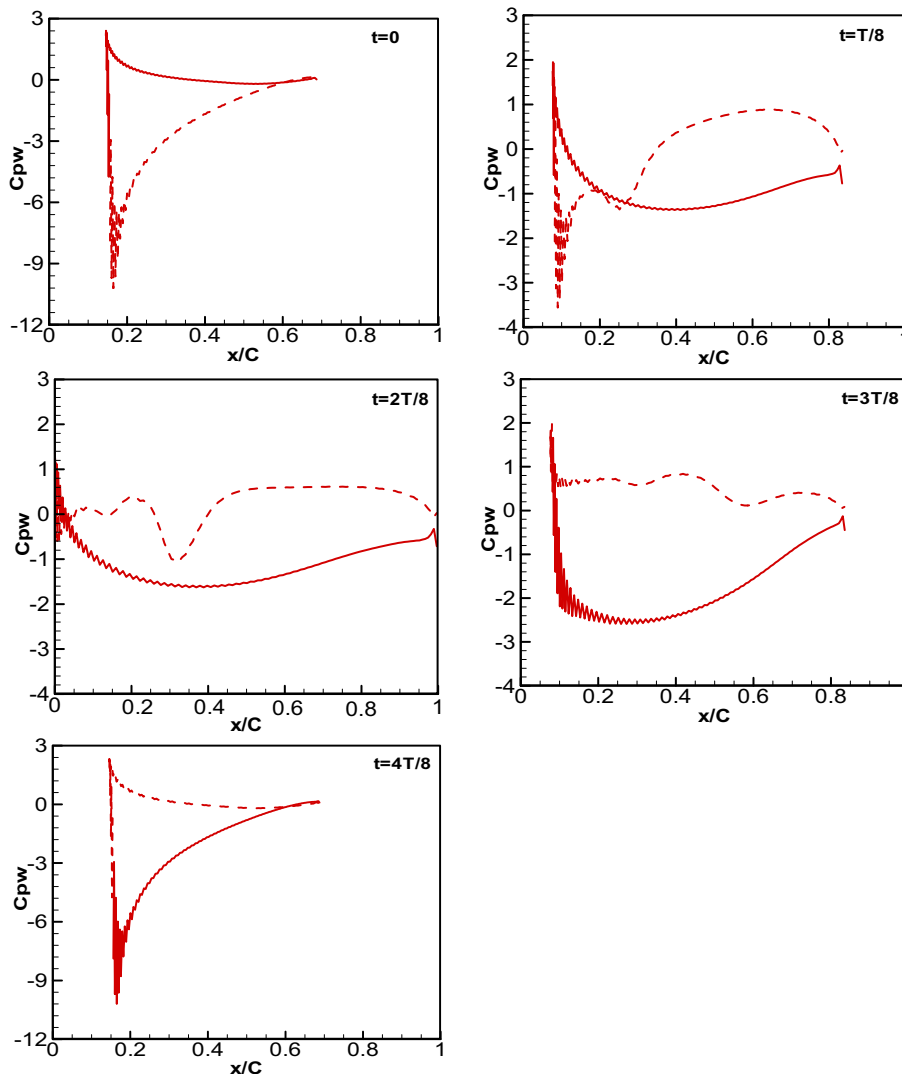

Fig. 13. Instantaneous wall pressure distribution within one period at $\beta = 1.0$ with $St = 0.35$ and $\alpha_0 = 10°$. Solid line: lower wall pressure; Dashed line: upper wall pressure.

The evolution of instantaneous vorticity contours in half a cycle is shown in Figs. 10–12 for $\beta = 1.0$, 1.5 and 4.0, respectively, with $St = 0.35$ and $\alpha_0 = 10°$. Note that the contours in another half cycle are inverse symmetric to the ones in this half cycle, because of the analogous property of the flapping motion profile. Taking a close-up observation, we can find the general evolution process of the vortices for different β. It is seen that a leading edge vortex (LEV) starts to form around at $t = 0$ where the pitching angle reaches its maxima and the plunging velocity has the maximum value as well. The LEV continues its growth and becomes the strongest at $t = 1/4\,T$ among these snapshots. Afterward, the vortices originated near the leading edge interact with the rest part of the foil before shedding into the wake. When the LEV evolves along with the airfoil upper surface, a region with low pressure is generated as shown from Figs. 13–15 where the snapshots of surface pressure distribution at the corresponding instants over half a cycle are displayed. With the evolution of LEV, a local minima of the pressure occurs on the upper surface indicating that the vortex moves from leading edge to trailing edge. At $t = 1/4\,T$, the vortex reaches its highest strength and consequently, leads to the largest negative changes on upper surface pressure as shown in the pressure distributions at this instant.

Note that the surface pressure distribution has profound contribution to the lift force C_L and pitching moment C_M which are directly related to the output power coefficient. We discuss its impact on the C_L first.

Based on the observations from Figs. 10–15, we can see that the pressure distribution are essentially determined by the amplitude and direction of the effective angle of attack which is significantly affected by β. For different β shown here, it is found that upper wall pressure is always larger than lower wall pressure at the interval from 0.25 T to 0.5 T which basically corresponds to the negative effective angle of attack (α_{eff} in Fig. 3). This indicates that the negative AOA generally results in negative (i.e., downwards) lift forces ($C_L < 0$) during the foil oscillating process. Although the LEV becomes stronger with β increasing, it seems that the LEV does not have essential impact on the pressure distributions discussed above. During the interval from 0.25 T to 0.5 T, it should be noted that, the airfoil has also a downwards plunging velocity (i.e. $dh/dt < 0$) as revealed from Fig. 2. Clearly, a positive product $C_L \cdot dh/dt$ is obtained exhibiting that the surface pressure forces during this interval contribute positively to energy extraction. Obviously, it is also true for the contribution of the surface pressure at the interval from 0.75 T to T due to the inverse symmetry. This is the reason why lift forces generally offer positive contribution to the energy extraction as we observed in previous discussions.

At the same time, the surface pressure forces definitely have essential effect on the pitching moment coefficient C_M as well.
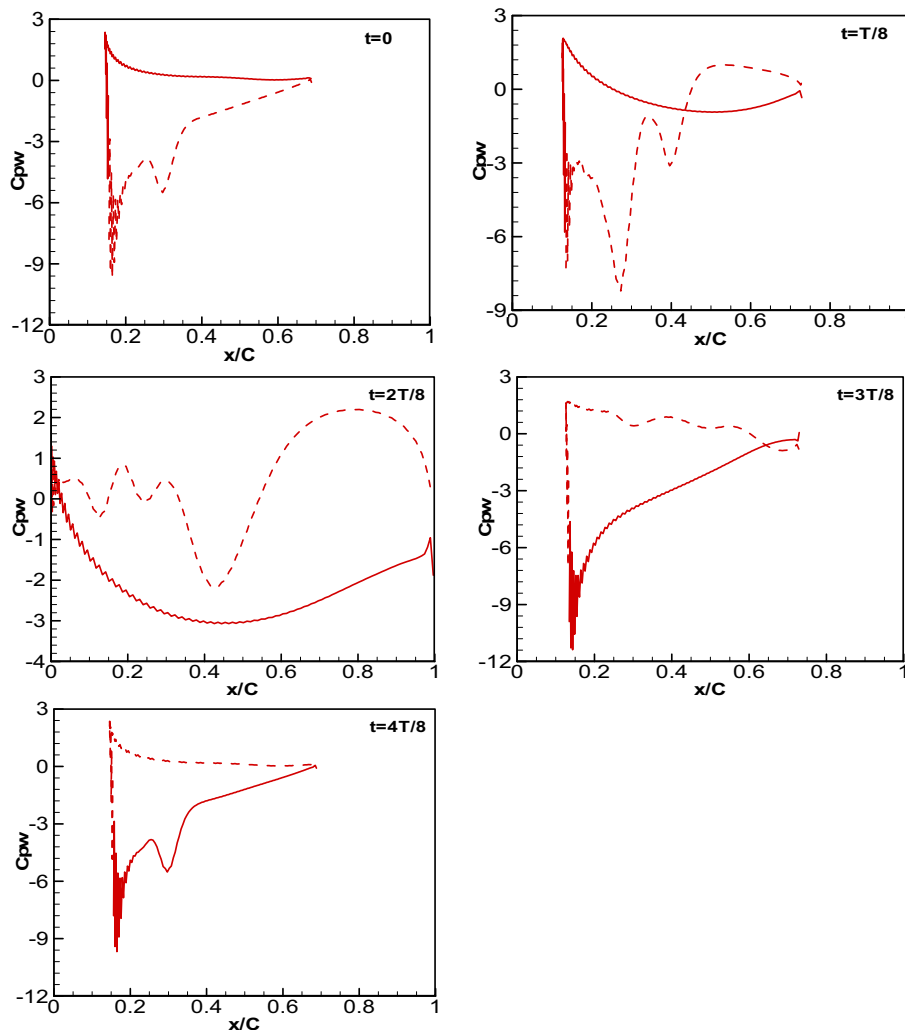

Fig. 14. Instantaneous wall pressure distribution within one period at $\beta = 1.5$ with $St = 0.35$ and $\alpha_0 = 10°$. Solid line: lower wall pressure; Dashed line: upper wall pressure.
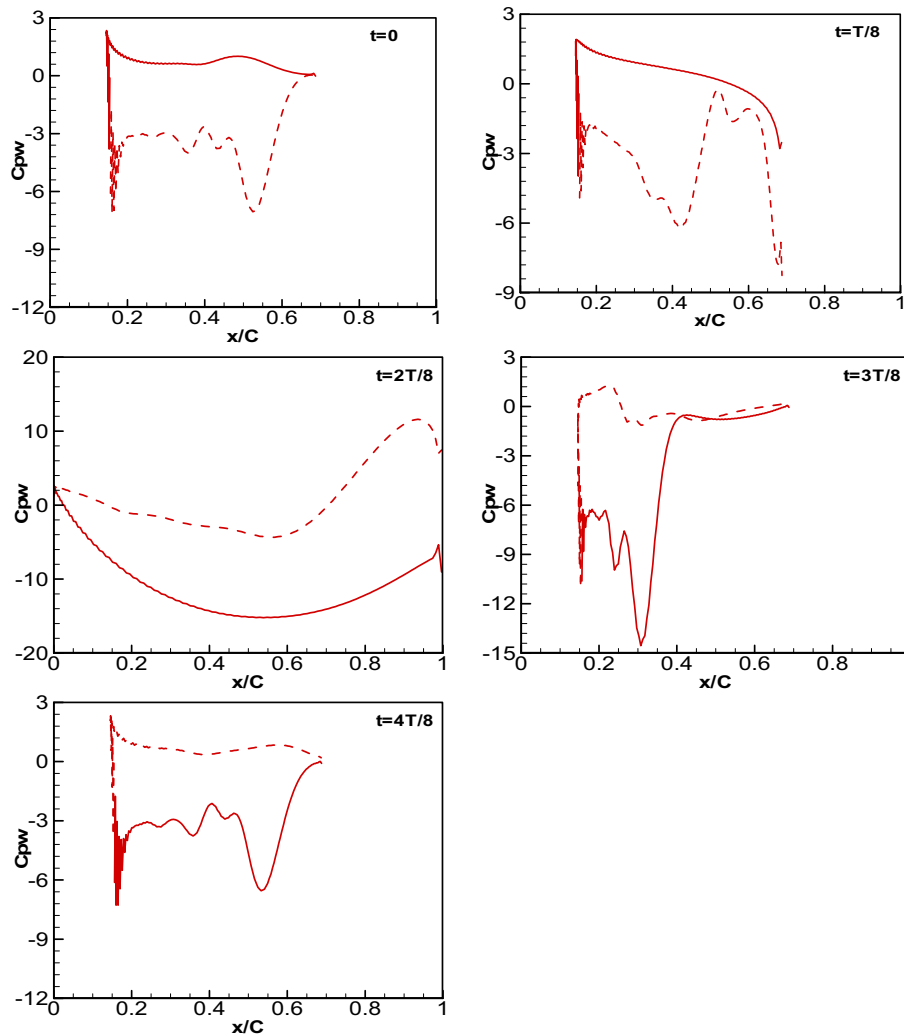
Fig. 15. Instantaneous wall pressure distribution within one period at $\beta = 4.0$ with $St = 0.35$ and $\alpha_0 = 10°$. Solid line: lower wall pressure; Dashed line: upper wall pressure.

Among all eight snapshots (five of them shown in Figs. 13—15) discussed here, their pitching angles are fixed at the maximum value for $\beta > 1$ except the instants $t = 0.25\,T$ and $t = 0.75\,T$ (i.e. $\theta = \pm\,\theta_0$ and $d\theta/dt = 0$). That means those C_M have no contribution to the output power due to $C_M \cdot d\theta/dt = 0$ at these instants. Noting that the pitching axis lies at $x = c/3$, we know, therefore, at the instant $t = 0.25\,T$, the moment caused by the pressure force is clockwise opposite to the direction of pitching motion. The similar situation is observed at the instant $t = 0.75\,T$. Meanwhile, the magnitude of pitching velocity $d\theta/dt$ reaches their maximal values at $t = 0.25\,T$ and $t = 0.75\,T$. Thus, the moment given by the product of C_M and $d\theta/dt$ during the intervals around $t = 0.25\,T$ and $t = 0.75\,T$ dominate the whole cycle and thus make significant negative contribution to the energy extraction, which has been observed and verified by the profiles of the instantaneous total output power coefficient and its two components contributed by lift force and pitching moment shown in Figs. 8 and 9.

4. Conclusions

This numerical study examines the potential of energy extracted oscillating foil to enhance the output power and efficiency with a non-sinusoid pitching motion combined with the sinusoidal plunging. The investigation covers a wide range of St and effective angle of attack. A specially proposed trapezoidal-like pitching profile is investigated, with the portion of flatten $\theta = \pm\,\theta_0$ being adjustable in each oscillating cycle, via a controlled parameter β. With $\beta > 1.0$ and $St < St_c$, the time-mean output power coefficient over one cycle is shown to increase significantly compared to the counterpart of $\beta = 1.0$ corresponding to the sinusoidal pitching. Similar trend is also observed with overall efficiency. The extension of St_c to higher value and increment of maximal C_{op} and η_T depend considerably on β as well as the oscillating system kinematic parameters. For a given nominal angle of attack α_0 and plunging amplitude h_0, there exists an optimal β at which the maximum power output significantly increases, generally along with a profound increase of St_c.

Further examination is focused on the analysis of how flow structure, lift force coefficient C_L, plunging velocity dh/dt, momentum coefficient C_M and pitching angular velocity $d\theta/dt$ are altered by the change of β. The total output power coefficient is therefore decomposed into two components i.e. C_{p1} and C_{p2}. It is found that, C_{p1} which is the product of C_L and dh/dt increases with β, and always gives a positive contribution to energy output C_{op}, as in the most portion of a cycle C_L and dh/dt have the same sign. Meanwhile, β increasing also leads to the increase of C_M and $d\theta/dt$. However, they always have the opposite sign in one cycle, resulting in a negative contribution from C_{p2} to C_{op}. When β is slightly larger

than 1, the negative contribution from C_{p2} is smaller than the positive one from C_{p1}. However, with β becoming far beyond 1, C_{p2} increases much faster than C_{p1}. Thus, an optimal β exists somewhere for the best performance of energy extraction. For the kinematic parameters studied here, the optimal value is around $\beta = 1.5$.

Although the computations are based on the prescribed pitching and plunging motions and we are aware that this approach decouples the dynamic response of device to the unsteady loading which will be our next task in the on-going project, we believe that above conclusions are crucial for the understanding of physical mechanism on energy extraction devices from a hydrodynamic perspective and thus can provide vital guideline to the engineering design of the motion trajectory for similar devices.

References

[1] Kerr D. Marine energy. Philos Trans Royal Soc A 2007;365:971–92.
[2] Bryden IG, Grinsted T, Melville GT. Assessing the potential of a simple tidal channel to deliver useful energy. Appl Ocean Res 2004;26:198–204.
[3] Westwood A. Ocean power wave and tidal energy review. Refocus 2004;5: 50–5.
[4] Triantafyllou MS, Techet AH, Hover FS. Review of experimental work in biomimetic foils. J Ocean Eng 2004;29:585–94.
[5] Stingray tidal stream energy device – Phase 3 2006 The Engineering Business Ltd, Report T/06/00218/00/REP.
[6] Platzer MF, Bradley RA. Oscillating-wing power generator with flow-induced pitch-plunge phasing. IPC8 Class: AF03D900FI USPC Class: 290 55 US Patent.
[7] McKinney W, DeLaurier J. The wingmill: an oscillating-wing wind-mill. J Energy 1981;5:109–15.
[8] Anderson JM, Streitlien K, Barrentt DS, Triantafyllou MS. Oscillating foils of high propulsive efficiency. J Fluid Mech 1998;360:41–72.
[9] Lewin GC, Haj-Hariri H. Modelling thrust generation of a two-dimensional heaving airfoil in a viscous flow. J Fluid Mech 2003;492:339–62.
[10] Hover FS, Haugsdal O, Triantafyllou MS. Effect of angle of attack profiles in flapping foil propulsion. J Fluids Struct 2004;19:37–47.
[11] Xiao Q, Liao W. Numerical investigation of angle of attack profile on propulsion performance of an oscillating foil. Comput Fluids 2010;39:1366–80.
[12] Xiao Q, Liao W. Numerical study of asymmetric effect on a pitching foil. Int J Mod Phys C 2009;20:1663–80.
[13] Davids ST. A computational and experimental investigation of a flutter Generators. M.S. dissertation, Naval Postgraduate School 1990.
[14] Jones KD, Platzer MF. Numerical computation of flapping-wing propulsion and power extraction; 1997. AIAA Paper 97–0826.
[15] Jones KD, Lindsey K, Platzer MF. An investigation of the fluid-structure interaction in an oscillating-wing micro-hydropower generator. In: Chakrabarti Brebbia, Almorza Gonzalez-Palma, editors. Fluid structure interaction, vol. 2. Southampton, England, U.K: WIT Press; 2003. p. 73–82.
[16] Kinsey T, Dumas G. Parametric study of an oscillating airfoil in a power-extraction regime. AIAA J 2008;46:1318–30.
[17] Simpson BJ, Hover FS. Triantafyllou MS. Experiments in direct energy extraction through flapping foils. Proc The Eighteenth International Offshore and Polar Engineering Conference, Canada, July 6–11, 2008.
[18] Zhu Q, Peng ZL. Mode coupling and flow energy harvesting by a flapping foil. Phys Fluids 2009;21:033601.
[19] Zhu Q, Haase M, Wu CH. Modeling the capacity of a novel flow-energy harvester. Appl Math Model 2009;33:2207–17.
[20] Zhu Q, Peng ZL. Energy harvesting through flow-induced oscillations of a foil. Phys Fluids 2009;21:123602.
[21] Shimizu E, Isogai K, Obayashi S. Multiobjective design study of a flapping wing power generator. J Fluids Eng 2008;130:021104–18.
[22] Jameson A, Schmidt W, Turkel E. Numerical solutions of the Euler equations by finite volume methods using Runge-Kutta time-stepping schemes. AIAA Paper 81–1259, AIAA 14th Fluid and Plasma Dynamic Conference, Palo Alto, June 1981.
[23] Turns SR. Thermodynamics: concepts and applications. Cambridge University Press; 2006.
[24] Chung TJ. Computational fluid dynamics. Cambridge University Press; 2002.